Passive Freezing Desalination driven by Radiative Cooling

Xin Huang, Jyotirmoy Mandal, Jin Xu and Aaswath P. Raman*

¹Department of Materials Science and Engineering, University of California, Los Angeles, CA 90024, USA

*Corresponding Author: <u>aaswath@ucla.edu</u>

Abstract

With increasing water scarcity there is now significant interest in finding lower-cost ways to generate fresh water. At the same time, many industrial processes, including oil and gas production, produce high-salinity wastewater that requires remediation. Conventional desalination processes, including membrane-based and thermal desalination approaches, require large energy inputs which can become prohibitive as salinity increases. Alternatively, the most commonly used passive thermal desalination method is solar desalination which uses the sun as the heat source in an evaporation-condensation cycle. However, weather conditions and solar insolation limit its applicability throughout the year. Here, we propose a passive approach to a more thermodynamically attractive phase change that can also enable desalination: freezing. In particular, we use the ultimate heat sink, outer space, through radiative cooling to enable passive freezing desalination. We experimentally demonstrate passive desalination of 37.3 g/L salt water to 1.88 g/L after two radiative cooling-driven freezing desalination stages, with 50% recovery and 17.5 g/L salt water to 0.7 g/L after two radiative cooling-driven freezing desalination stages, with 65% recovery. We develop and validate a thermal model that accurately predicts the performance of the system and extend it to probe the theoretical limits of performance. These results demonstrate that passive freezing desalination driven by radiative cooling could fundamentally enable new technological possibilities for desalination. Further, this could be a complementary method to solar desalination to enable 24-hour, year-round passive thermal desalination.

Introduction

Freshwater scarcity is expected to grow with rising temperatures this century, a challenge that will be compounded by growth in demand for water worldwide¹. Only 1.5% of water on Earth is freshwater, with 96.5% of total water on earth in the ocean as saltwater². Desalination has thus become an important method for the production of fresh water with daily desalination capacity estimated as 95.37 million m³/day at the end of 2018³, twice the rate of global water production in 2008⁴. In addition to fresh water generation, managing industrial waste streams including saline waste from oil and gas facilities⁵-7 as well as brine waste³ from seawater desalination plants, is essential to mitigate the threats they pose to human health³ and environmental conditions¹¹⁰. Conventional membrane-based desalination processes are widely deployed but require significant energy inputs¹¹¹-¹³. Collectively, most desalination systems today demand substantial energy intensity, and thus lie at the heart of the nexus between energy and water use.

Thermal desalination has been actively explored for decades as a mechanism to complement reverse osmosis-based systems and is today a commonly used method for desalinating high salinity waters and brines. Thermal desalination entails the evaporation of salt water and its condensation into pure water, with typical thermal desalination systems also demanding large energy inputs typically driven by non-renewable fuels^{14–17}. One notable exception is solar desalination^{18,19}, which exploits a renewable source of energy, and in the past decade has seen substantial advancement in systems enabled by solar-driven interfacial evaporation^{20,21}. Although much work has gone into developing high-performance materials^{22–28} and high-efficiency system designs^{29–32} solar desalination's need for high solar insolation has placed limits on its applicability in many geographic regions. Furthermore, the use of evaporation, a high-temperature phase change, introduces additional operational costs due to scaling and corrosion.

Here, we focus on an alternate phase change that can also enable thermal desalination: freezing. Freezing desalination exploits the fact that when water is crystallized to ice, salt will separate from the ice crystals which will be pure water. Compared to evaporation, the energy needed for the phase change can be reduced by 75% to 90% as the latent heat of fusion of ice is 334 kJ/kg, in contrast to the heat of evaporation of water which is 2256 kJ/kg at 100°C³³. Experiments in the 17th and 18th centuries demonstrated freshwater generation through the freezing of sea ice^{34–36}. In the modern era, freezing desalination has remained an active topic of research inquiry with considerable focus on improving its efficiency^{37–43}. Despite substantial early

work on freezing desalination in the 1960s, commercialization of the technology has been hampered due to the substantial energy input needed for the freezing process⁴⁴. If freezing desalination were possible to enable passively, however, its viability as a technology might be dramatically enhanced. Moreover, it could complement existing thermal evaporative desalination methods, including solar desalination.

Given this context, we are motivated by recent breakthroughs in passive radiative cooling^{45,46} wherein sky-facing surfaces radiate their heat as thermal radiation, some of which effectively escapes to the cold of space through an atmospheric window in the long-wave infrared part of the electromagnetic spectrum between $8-13 \mu m$. To passively reach temperatures substantially below the ambient, as one would need for freezing, it is well understood that thermal emitters that selectively emit within the atmospheric window will outperform broadband emitters^{47–49}. Prior work has shown that with a selective emitter and a vacuum system to minimize non-radiative heat gain a maximal reduction of 42 °C relative to the ambient is achievable⁴⁶. Because of its cooling performance below ambient temperature, radiative coolers have also been used to obtain dew from atmosphere⁵⁰. In the context of desalination, a single observational study in 1974 claimed that a natural freezing process resulted in desalination in open pools of salt water in the Atacama desert in Chile, where both evaporative and radiative cooling nominally resulted in freezing desalination⁵¹. However, this work did not provide any quantitative data with respect to the salinity levels of the water generated, and the overall efficiency of the process. Since that early work, no further attempts have been made at enabling a passive thermal desalination process using freezing, while on the other hand substantial research interest has continued in solar thermal desalination. Moreover, recent advances in optimizing radiative cooling materials raise the intriguing possibility that this passive cooling mechanism could enable a compelling technological capability for thermal desalination.

In this article, we conceptually develop, and experimentally demonstrate passive freezing desalination driven by radiative cooling. Furthermore, we develop and validate models against our experimental results and use them to model expected performance in a range of climate zones, and also explore the thermodynamic limits of performance of this approach to desalination. Collectively, our work shows that passive freezing desalination can be both competitive and complementary to solar desalination, and other thermal desalination approaches.

Conceptual Overview

Fig. 1(a) shows the overall concept of the radiative cooling-driven freezing desalination process we propose. A sky-facing radiative cooler passively freezes the saltwater and ice, which in turn separate, with remaining higher salinity brine sinking because of its higher density. The generated ice can then be melted into pure water. Fig. 1(b) shows the specific steps in the radiative cooling-driven freezing desalination process. After freezing the salt water by thermal contact with the radiative cooling surface, the ice and the brine are mechanically separated through a simple filter. In practice, the remaining ice will have saltwater pockets trapped within it. Thus, following standard processing techniques for freezing desalination, we wash the generated ice particles with a small volume of pure water. The remaining high-purity ice is then melted to obtain fresh water.

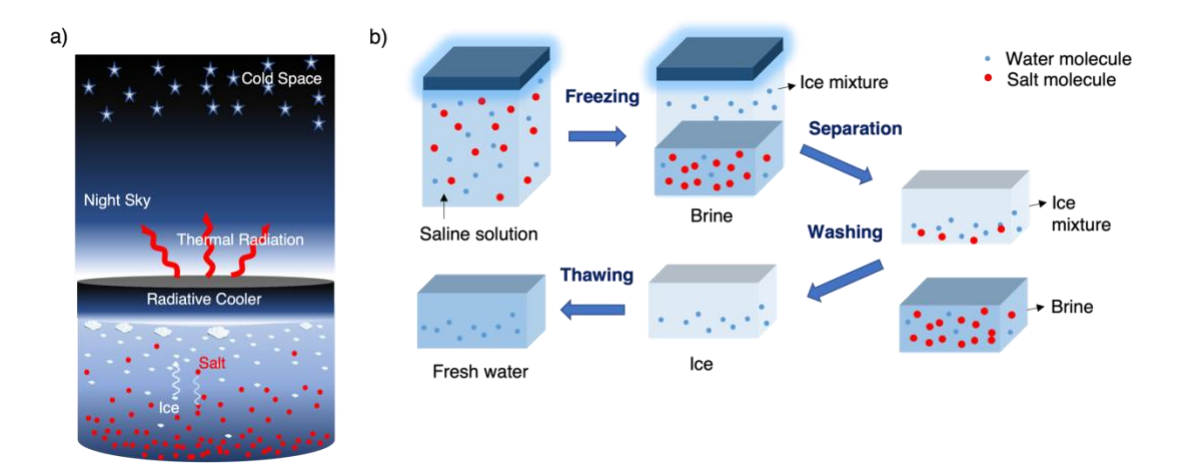


Figure 1: a) Conceptual framework of the radiative cooling freezing desalination process. The ice forms inside the salt water because of the coldness of the radiative cooler and separates with the brine. **b)** Detailed schematic of a single stage freezing desalination process, including freezing, separating, washing and melting.

We now examine the basic heat transfer mechanisms at play here to understand the potential of this passive approach to desalination. Consider a radiative cooler of area A at temperature T. When the radiative cooler is exposed to the night sky, it is subject to downwelling atmospheric thermal irradiance (corresponding to ambient air temperature T_{amb}) as well as non-radiative heat exchange to its surroundings. The net cooling power P_{net} achievable by the radiative cooler is given by:

$$P_{net}(T) = P_{rad}(T) - P_{atm}(T_{amb}) - P_{cond+conv}$$
 (1)

In Eq. (1) the power radiated out by the radiative cooling surface is

$$P_{rad}(T) = A \int d\Omega \cos \theta \int_0^\infty d\lambda I_{BB}(T,\lambda) \, \epsilon(\lambda,\theta) \tag{2}$$

Here $\int d\Omega = 2\pi \int_0^{\frac{\pi}{2}}$ is the angular integral over a hemisphere. $I_{BB}(T,\lambda) = \frac{2hc^2}{\lambda^5} \frac{1}{e^{hc/(\lambda k_B T)} - I}$ is the spectral radiance of a blackbody at temperature T, where h is Planck's constant, k_B is the Boltzmann constant, c is the speed of light and λ is the wavelength.

$$P_{atm}(T_{amb}) = A \int d\Omega \cos\theta \int_0^\infty d\lambda I_{BB}(T_{amb}, \lambda) \epsilon(\lambda, \theta) \epsilon_{atm}(\lambda, \theta)$$
 (3)

is the absorbed downwelling atmospheric irradiance over long-wave infrared wavelengths. The atmospheric emittance $\varepsilon_{atm}(\lambda)$ is calculated from $I_{sky}(\lambda)$ using the MODTRAN Web Application for different weather conditions, as shown in the Supplementary section. Finally, heat gained due to conduction and convection $P_{cond+conv}$ can be expressed based on a combined effective heat transfer coefficient h_c as

$$P_{cond+conv}(T, T_{amb}) = Ah_c(T_{amb} - T). (4)$$

A selective thermal emitter will have high emittance within the atmospheric window (8–13 µm) and low emittance elsewhere. For below-ambient cooling (i.e., $T < T_{amb}$), a broadband thermal emitter stands to gain more heat from thermal radiation outside the atmospheric window than it loses through thermal emission within the window, potentially resulting in negative cooling power and limiting the lowest temperature achievable. By contrast, a selective emitter allows us to maximize $P_{net}(T)$ at sub-ambient temperatures and thereby achieve a lower temperature, which is essential for freezing desalination.

At the onset of freezing, the maximum ice generation rate that can be formed from simple thermodynamic considerations alone can be understood by equating the net cooling power P_{net} at

that temperature to v_f , the ice generation rate of salt water and H_f the enthalpy of fusion of water (334 kJ/kg):

$$P_{net}\left(T\right) = v_f H_f \tag{5}$$

To illustrate the potential of radiative cooling-driven desalination, we calculate and show in Fig. S1 the maximum ice generation rate per second at a temperature of -2°C for a range of air temperatures and relative humidity conditions assuming an ideal selective emitter. While this is meant to be a first-order thermodynamic approximation, it does indicate the potential of radiative cooling to enable meaningful ice generation for a range of weather conditions. In a full implementation of such a system, to enable truly passive operation, the radiative cooling surface will further be responsible for cooling the saline solution to the onset of freezing, and the kinetics of the freezing process will determine the nature of crystallization. We explore this in further detail as part of our experimental implementation and detailed modeling in this paper.

Experimental Implementation

We experimentally demonstrated passive freezing desalination driven by radiative cooling using a custom-built apparatus shown in Fig. 2(a). The radiative cooling surface is made of a low-cost acrylic polymer (3M Scotch tape⁵²) coated with silver, which is then affixed to a polished aluminum cold plate which contains two tubes for water. The plate and radiative cooling surface are placed inside a polystyrene box which is covered with Aluminized mylar both inside and outside to minimize its own emittance. Two clear 12.5-µm polyethylene films are placed above the sample at a distance of 7 cm as an infrared-transparent windshield to enable effective, yet low-cost insulation. Hemispherical emissivity measurements of the radiative cooling surface show that it possesses a selective thermal emittance with high emittance in the atmospheric window (Fig. 2(b)).

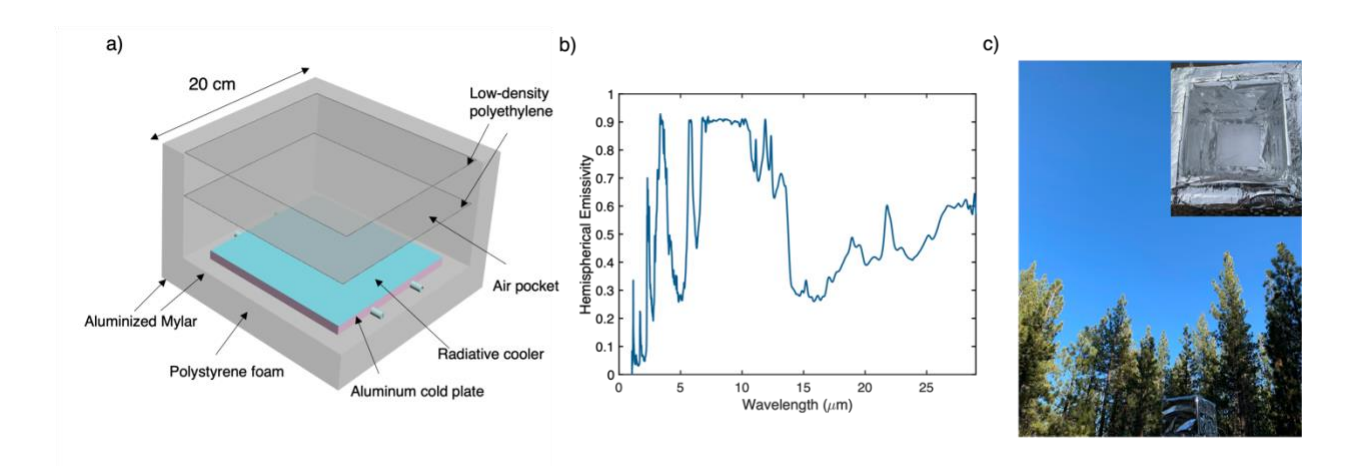


Figure 2: Experimental apparatus and conditions: (a) Three-dimensional schematic of the radiative cooling apparatus. A cold plate with two tubes is used to place the salt water in thermal contact with the radiative cooling surface, while the rest of the apparatus is designed to minimize conductive and convective heat exchange to the cooler. (b) Hemispherical emissivity measurement of the low-cost acrylic polymer used as the radiative cooling surface in the experiment. (c) Photo of the setup and its surroundings in Big Bear Lake, CA, USA. The apparatus can be seen at bottom during daylight hours. Experiments were conducted at night.

We demonstrated the performance of the radiative cooling desalination device in two overnight experiments at Big Bear Lake, California (photo of the environment is shown in Fig. 2(c)), by exposing it to the sky during night-time hours and testing its performance. In the first experiment, the tubes in the cold plate were filled with 30 mL of salt water at 37.3 g/L, approximately the salinity of seawater. As shown in the temperature data of Fig. 3(a), immediately after the cooler is exposed to the environment (shortly before 22:30 local time in Fig. 3(a)), its temperature drops to approximately 8°C below the measured ambient air temperature. The temperature of the saltwater reaches -6.2°C around 00:40 at which point it rises rapidly to -2.98°C, a signature of the onset of freezing. The temperature of the forming ice/water slurry then slowly drops to -4.5°C during the crystallization process. Through multiple lab experiments we determined that this temperature range resulted in approximately 75% crystallization in our setup, a crystallization level previously shown to be optimal for freezing desalination³⁷. At this point, we removed the ice/water and brine mixture from the tube and mechanically separate the ice and brine using a simple paper filtration system and use 3.5 mL of fresh water to wash the formed ice crystals to remove the attached brine on the surface of the ice crystal. 19 mL of water with a salinity of 8.99 g/L is obtained after melting the ice crystals, as shown in Fig. 3(c).

We then re-inserted the partially desalinated water from the first stage back into the tube of the cold plate and repeated the previous steps for a second stage of freezing desalination. As shown in the temperature data of Fig. 3(b), after the cooler is exposed to the environment (at 03:07 local time in Fig.3 (b)), its temperature drops to around -5°C at 04:00 and immediately rises to -1.35°C because of the lower salinity of the salt water. We repeated the separation process and used 2.5 mL of fresh water to wash the formed ice crystals. After the second stage's desalination process, we finally obtained 15 mL with a salinity of 1.88 g/L (Fig. 3(c)) representing a 50% recovery rate from the 30 mL salt water initially introduced into the system. We note that the wash water used in both stages rapidly flows past the ice and in this implementation contributes negligibly to the finally measured output water from the system which is determined by melting the remaining ice.

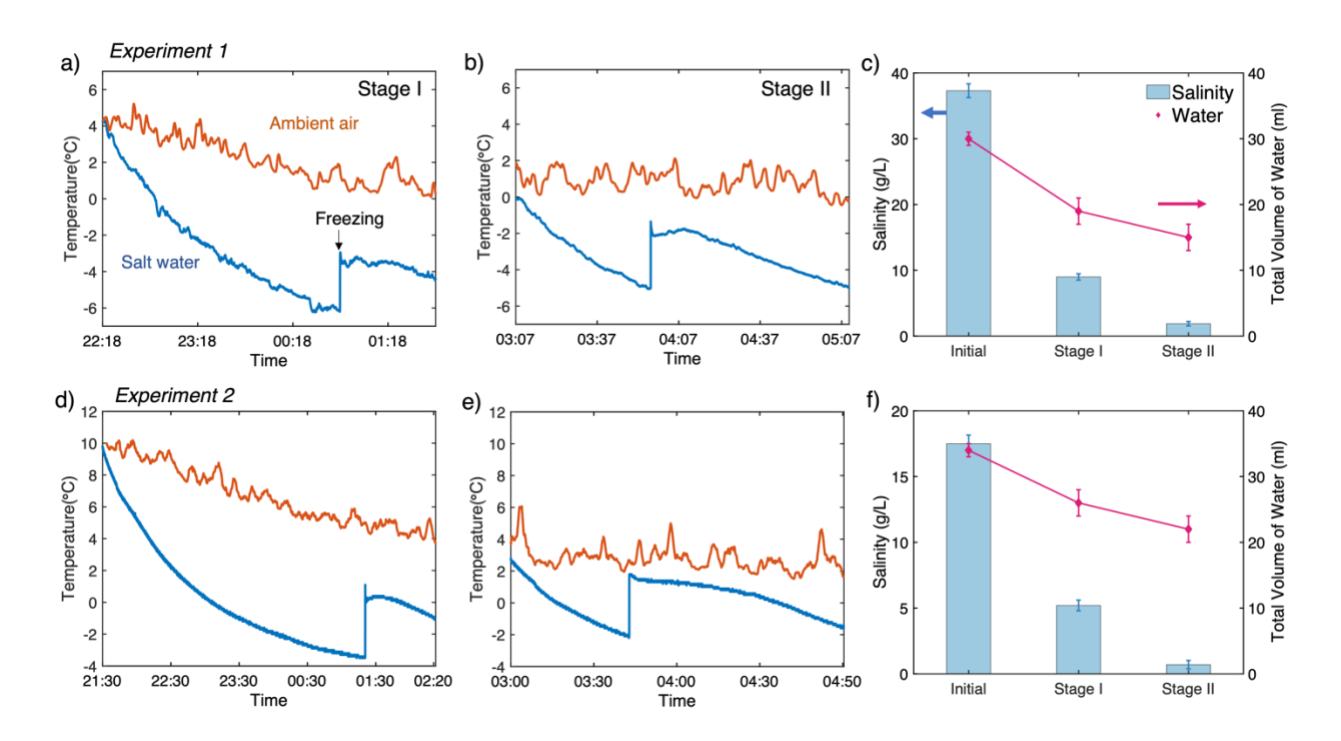


Figure 3: a) First stage measurement of the salt water (37.3g/L) temperature (blue) against ambient air temperature (orange) on a clear night in Big Bear Lake, California, USA. The water temperature immediately drops below ambient once exposed to the sky and increases from -6.2°C to -2.98 °C at the onset of freezing. **b)** Second stage measure of the first stage's saltwater temperature (blue) vs. ambient air temperature (orange). The water temperature drops to -5.01 °C and then rises to -1.35 °C at freezing onset. **c)** Salinity measurements of the two desalination stages. The salinity of water drops from 37.3 g/L to 8.99 g/L after the first stage with a 11 mL water loss and from 8.99 g/L to 1.88 g/L at the second stage with a 4 mL water loss. **d)** First

stage measurement of the lower salinity input saltwater (17.5 g/L) temperature (blue) vs. ambient air temperature (orange) on a clear night at the Big Bear Lake test site. The water temperature immediately drops below ambient once exposed to the sky and increases from -3.5°C to 1.1 °C at the onset of freezing. e) Second stage measurement of the saltwater temperature (blue) vs. ambient air temperature (orange). The water temperature drops to -2.2 °C and then rises to 1.65 °C at freezing onset. f) Salinity measurements after each desalination stage. The salinity of water drops from 17.5 g/L to 5.2 g/L at the first stage with an 8 mL water loss and from 5.2 g/L to 0.7 g/L at the second stage with a 4 mL water loss.

To explore the effect of initial input salinity, in a second experiment we demonstrated the performance of the radiative cooling desalination device for lower salinity input water. In this experiment, the tubes in the cold plate were filled with 34 mL of salt water at 17.5 g/L input salinity. As shown in the temperature data of Fig. 3(d), immediately after the cooler is exposed to the environment (at 21:30 local time), its temperature drops to approximately 13°C below the measured ambient air temperature, a deep sub-ambient cooling effect enabled by the selective thermal emitter. The temperature of the saltwater reaches -3.5°C at around 01:10 at which point it rises rapidly to 1.1°C at freezing onset. The temperature of the forming ice/water slurry then slowly drops to -1.2°C during the crystallization process. As in the previous experiment, we mechanically separated the ice and brine and used 3.5 mL of fresh water to wash the formed ice crystals to remove the attached brine on the surface of the ice crystal. 26 mL of water with a salinity of 5.2 g/L is obtained after melting the ice crystals, as shown in Fig. 3(f). We next re-inserted the 26 ml of 5.2 g/L salinity saltwater back into the tube of the cold plate and repeated the previous steps for a second desalination stage. As shown in the temperature data of Fig. 3(e), after the cooler is exposed to the environment (at 03:00 local time in Fig. 3(e)), its temperature drops to around -2°C at 03:45 and immediately rises to 2°C because of the lower salinity of the salt water. We then repeated the separation process and use 2.5 mL of fresh water to wash the ice crystals. After the second stage's desalination process, we finally obtained 22 mL of water at a salinity of 0.7 g/L (Fig. 3(f)) representing a 65% recovery rate from the 34 mL salt water initially introduced into the system.

After the first stage of the desalination process in these experiments the salinity of saltwater decreases 70-75% while there is also 8-11 mL water loss. Previous work has shown that in freezing desalination systems the removal efficiency decreases as the residual liquid volume reduces due to the difficulty of maintaining regular contact between the liquid and solid phases⁵³. Freezing in

general can further cause impurities to be trapped inside ice crystals relative to the fraction of the solution that remains unfrozen. This in turn can result in lower separation efficiency of the salt-water solution^{54–56}. There is thus a compromise between water loss and the purity of water obtained that we believe can be further optimized in future work. Finally, we note that the pump for the mechanical separation process used here consumes about 30 J during the desalination process. This corresponds to less than 0.5% of the total energy that would otherwise be needed to freeze 19 ml of salt water. This energy consumption is thus negligible relative to the effective energy savings made possible by the passive radiative cooling process.

Modeling and validation

We next developed a theoretical model for the developed freezing desalination system, validated it against the experimental measurements and then used it to predict the net freshwater yield of both current and future improved radiative-cooling freezing desalination systems in a range of climate zones. Given input environmental conditions (air temperature and dew point), as well as the mass of water in the system, the model first predicts the cooling curve for water in the radiative cooling apparatus (see Supplementary Information for details). In Fig. 4(a), the model's prediction for the temperature of the saltwater at an input salinity of 37.3 g/L for a range of nonradiative coefficients of heat exchange is compared against the first stage experimental data in Fig. 4(a) and the second stage in Fig. 4(b), showing excellent agreement. The temperatures of saltwater for the lower input salinity experiment (17.5 g/L) for both stages are also simulated by the model, and shown in Fig. 4(c) and 4d), also showing excellent agreement. The model then uses this information, as well as phenomenologically derived assumptions about when freezing onset occurs, and the associated temperature rise of the saline solution, to predict a range of expected freshwater production rates for a particular set of operating conditions (see Supplementary Information). The model's predicted range of freshwater production is shown in Fig. 4(e) and is validated against the values obtained experimentally showing excellent overall agreement.

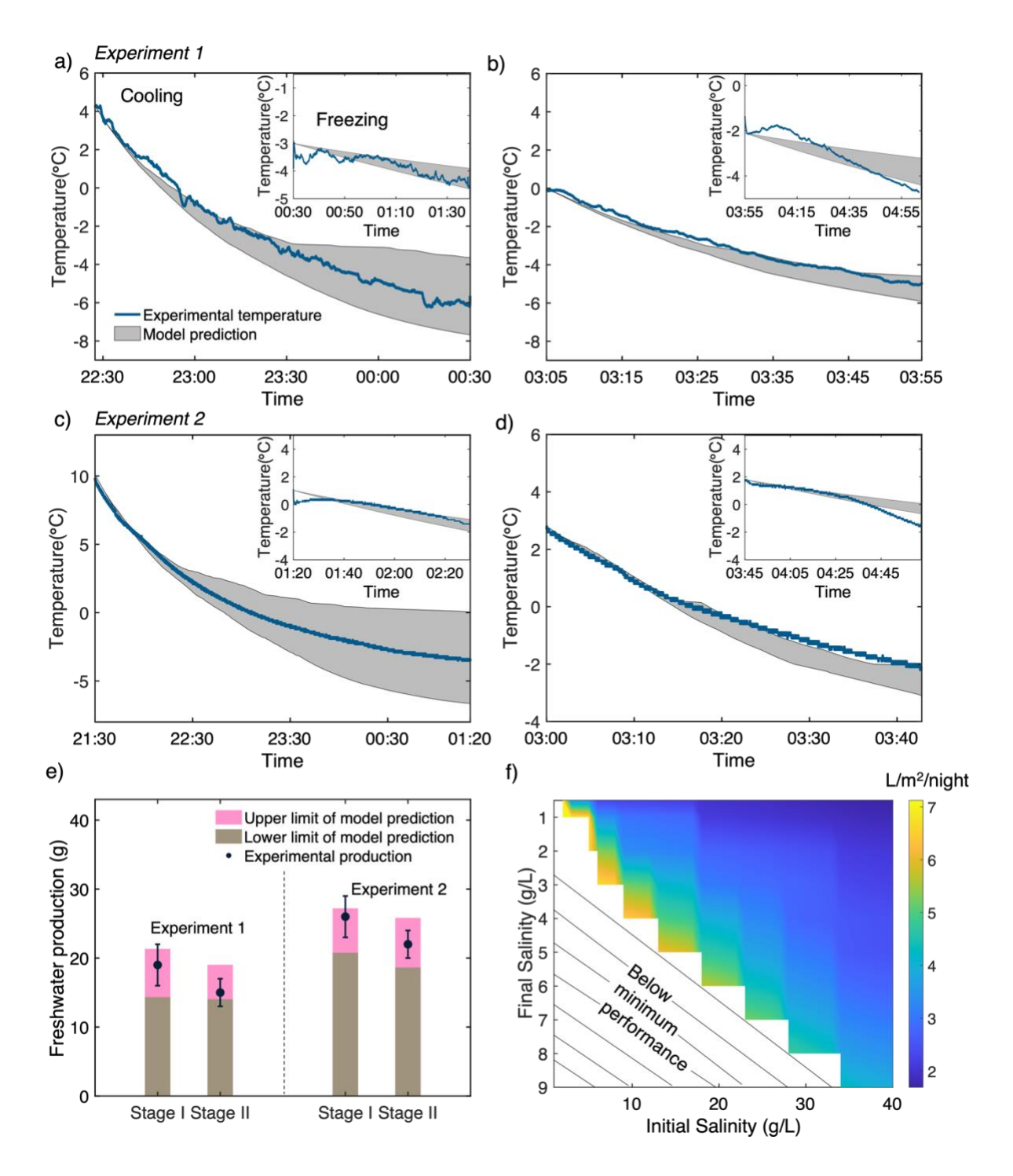


Figure 4: a) Model predictions (gray) vs. experimentally measured (blue) saltwater (37.3 g/L concentration) during the first stage, showing excellent agreement. The gray regions denote model uncertainty associated with the coefficient of non-radiative heat exchange which is modeled in a range of potential values. **b)** Model predictions (gray) vs. experimentally measured (blue) saltwater (37.3 g/L concentration) during the second stage, also showing good agreement. **c)** Model predictions (gray) vs. experimentally

measured (blue) saltwater (17.5 g/L concentration) during the first stage, showing excellent agreement. **d)** Model predictions (gray) vs. experimentally measured (blue) saltwater (17.5 g/L concentration) during the second stage, also showing good agreement. **e)** Modeled total freshwater production from saltwater vs. experimentally yielded quantities. **f)** Modeled total freshwater production using the experimental apparatus for different input salinities given weather conditions during experiments at the Big Bear Lake test site, and assuming the use of up to three consecutive stages.

We next used the validated model to predict the nightly freshwater output of our apparatus for different input and output salinities under the same set of environmental conditions as our experiments. First, we note that the higher the salinity of input saltwater, the harder it will be for it to freeze, as it will have to reach lower supercooling temperatures, as shown in Fig. S3. Furthermore, higher salinities can necessitate multiple stages of freezing and washing, as demonstrated in our experiments. Using our experimental implementation as a phenomenological baseline for the values of the input and output salinities achievable for experimental stage (with a maximum of four stages total set as an upper limit), we show in Fig. S5 the expected number of desalination stages needed as a function of input salinity. The model demonstrates that, given our apparatus and test environmental conditions, it takes at most three stages to desalinate freshwater from higher salinity water (37.3+ g/L), and takes fewer stages for lower input salinities. For seawater desalination (input salinity of 35 g/L), based on the current implementation (current cold plate, radiative cooling material and apparatus insulation) the performance of this system at different ambient temperatures and relative humidities is shown in Fig 5a. In this model, we assume that there is no supercooling resulting in freezing onset as prior works has shown that supercooling can be avoided by adding a nucleation agent or increasing the roughness of the nucleation surface^{54,57–61}.

Finally, to explore the performance limits of radiative cooling-driven freezing desalination, we further apply our model on an idealized freezing desalination system. We assume in this model that the mass of the cold plate is negligible, that the radiative cooling surface is under vacuum, that the radiative cooler is an ideal selective thermal emitter (with unity emissivity between 8-13 um and 0 at other wavelengths), that the convective shield has perfect transmittance and that there is no supercooling resulting in freezing onset exactly at the freezing point of 35 g/L salt water (-2 °C). The performance predictions under these assumptions for different ambient temperatures and relative humidities is shown in Fig. 5(b). For the ideal case, as much as 0.9 L/m²/h freshwater can

be generated using this method, which compares favorably with common solar desalination production values of 0.3-0.7 L/m²/h under the standard one Sun illumination condition $(1 \text{ kW/m}^2)^{62-64}$, but is lower than the theoretical limit of hourly averaged production values for a multi-stage solar desalination system, $10 \text{ L/m}^2/h^{15}$.

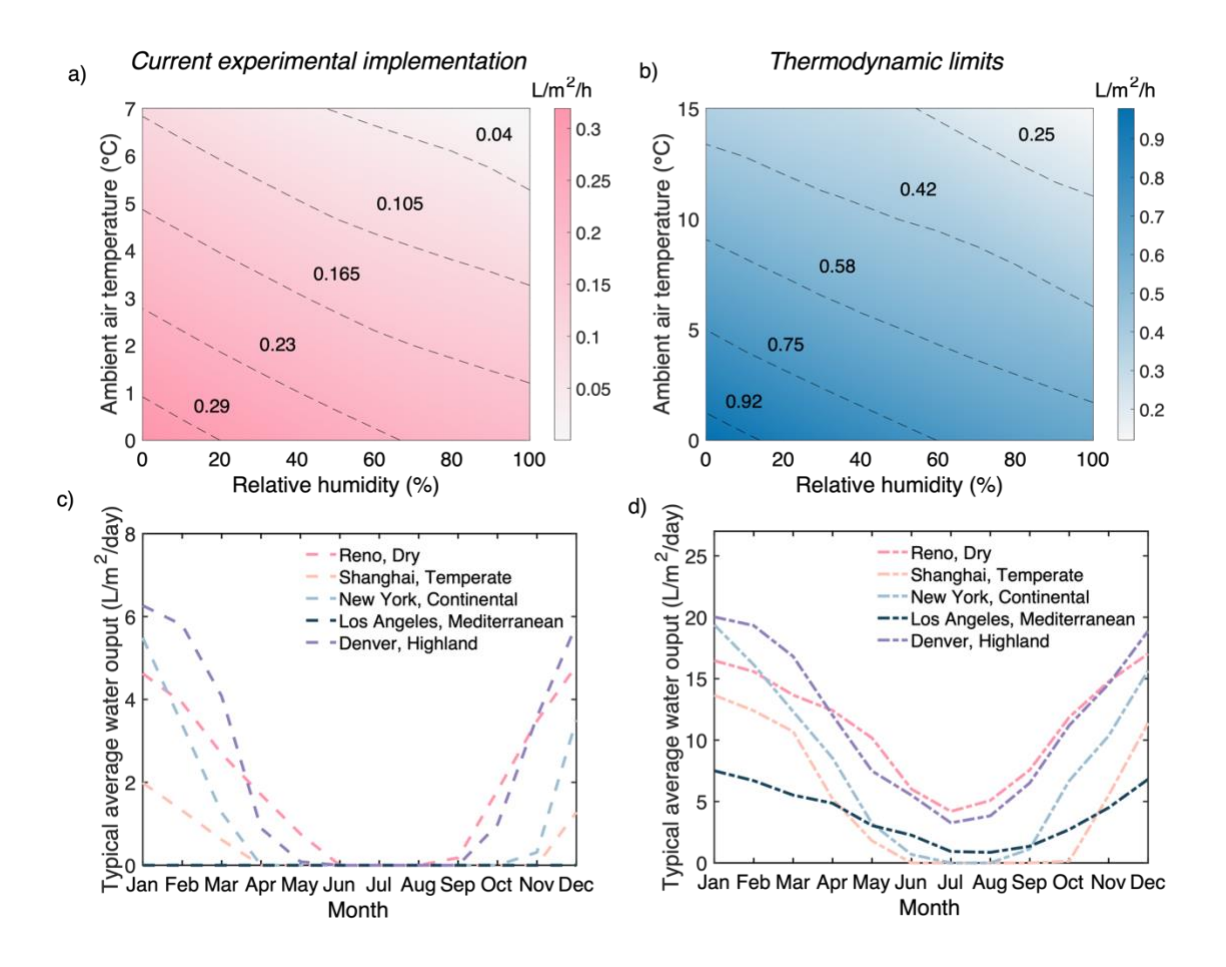


Figure 5: a) Model prediction of the amount of water produced hourly by radiative cooling freezing desalination assuming the current experimental implementation for different relative humidity and ambient temperatures. **b)** Single-state thermodynamic limit of hourly water production by radiative cooling freezing desalination for different relative humidity and ambient temperatures. **c)** Prediction of average daily water production each month of the current experimental implementation using typical meteorological year (TMY3) weather data for cities located in five different climate zones. **d)** Single-state thermodynamic limit of average daily water production each month for the same cities located in five different climate zones.

To further explore the viability of this approach to desalination, we apply our model using typical meteorological year (TMY3) data for cities in five different climate zones: dry, temperate,

continental, Mediterranean, and highland climates. We then calculate the amount of water produced by radiative cooling freezing desalination daily based on both the current experimental implementation in Fig. 5(c), as well as the production from the ideal passive radiative cooling-driven freezing desalination system in Fig. 5(d). In all cases we consider solar energy absorption by the radiative cooler based on its current solar reflectivity. Overall, with this desalination approach we observe the highest production during non-summer months when solar irradiance and ambient temperatures are cooler in all climate zones. However, as shown in Fig. 5(d), with further improvements meaningful production can occur during low solar irradiance hours in the summer as well. As can be seen in Table S2 of the Supplementary Information, the dry and highland climate zones are optimal climate zones due to many hours of relatively cooler air temperatures and lower relative humidities. However, in winter months with relatively solar irradiance, this approach may outperform solar desalination-based approaches.

While Fig. 5 examines the system's performance in terms of production capacity, the rates shown here must be compared against system costs. As a preliminary effort to that end, we developed a first order levelized cost of water (LCW) analysis for the passive freezing desalination system and benchmarked it against LCW ranges for other desalination methods. As shown in Fig. S6, production rates of 2-5 L/m²/day, achievable with the system as it would currently performs in range of climate zones (Fig. 5c), could yield LCW in the range $1.5 - 0.75/m^3$, competitive with solar desalination today⁶⁵. We note that with the theoretical limits of performance shown in Fig. 5(d), Fig. S6 indicates that LCW could be achieved that would be competitive with membrane desalination systems in a range of climate zones. The current implementation's costs are driven by small-volume manufacturing of the cold plate used, as well as sub-optimal performance due to non-ideal infrared selectivity as well as supercooling. Improvements on both these fronts are possible with increased manufacturing scale, as well as through further advancements in selective radiative coolers. While this is a preliminary estimate, the results do highlight the potential of this approach to desalination, given the simplicity of the system's components and low-temperature operation relative to alternate thermal desalination approaches that rely on evaporation. For climate zones with relatively low solar irradiance during large fractions of the year, radiative coolingdriven desalination may represent a compelling renewable thermal desalination approach, including to remediate saline wastewater in industrial, and oil and gas facilities.

Conclusion

To summarize, we have highlighted the remarkable possibility and potential of desalinating salt water by radiative cooling-driven freezing desalination. Unlike membrane desalination, our approach is passive and can in principle work for water of any salinity level. Compared with solar desalination, our approach overcomes both challenges associated with evaporative desalination, including corrosion related to high temperature operation, and makes freezing desalination more attractive from an energy input perspective. While a potentially competitive technology in its own right, we emphasize that radiative cooling-driven freezing desalination could be combined with solar desalination to realize year-round, 24 hour a day passive thermal desalination for the first time. The low-salinity water generated by this method could also serve as a preliminary stage for conventional membrane-based desalination to overcome the high pressures that can be encountered when desalinating high-salinity input streams. While radiative cooling has emerged in recent years as an important frontier for research in energy challenges, this work highlights the important contributions that harnessing the thermodynamic resource of the cold of space could play for water challenges we face this century.

Acknowledgements

This work was supported by the National Science Foundation (NSF CAREER) under Grant No. 2146577, the Sloan Research Fellowship (Alfred P. Sloan Foundation), and the Hellman Fellows Award. J.M. was supported by Schmidt Science Fellows, in partnership with the Rhodes Trust.

Author contributions

A.P.R. originated the concept and supervised the work. A.P.R. and X.H. conceived of and designed the experimental implementation. X.H. conducted and analyzed experiments. J.M. fabricated the radiative cooler and provided advice on the experiment. X.H. developed the theoretical model and J.X. provided advice on the thermal modeling. X. H. and A.P.R. wrote the original draft, J.M. reviewed and edited the manuscript.

Declaration of interests

A provisional patent (U.S.63/363,700) has been filed related to this work.

References

- 1. Shannon, M.A., Bohn, P.W., Elimelech, M., Georgiadis, J.G., Mariñas, B.J., and Mayes, A.M. (2008). Science and technology for water purification in the coming decades. Nature 452, 301–310.
- 2. Water in Crisis Paperback Peter H. Gleick Oxford University Press //global.oup.com/ushe/product/water-in-crisis-9780195076288.
- 3. Jones, E., Qadir, M., van Vliet, M.T.H., Smakhtin, V., and Kang, S. (2019). The state of desalination and brine production: A global outlook. Sci. Total Environ. *657*, 1343–1356.
- 4. Schiermeier, Q. (2008). Water: Purification with a pinch of salt. Nature 452, 260–261.
- 5. Vidic, R.D., Brantley, S.L., Vandenbossche, J.M., Yoxtheimer, D., and Abad, J.D. (2013). Impact of Shale Gas Development on Regional Water Quality. Science *340*.
- 6. Brantley, S.L., Vidic, R.D., Brasier, K., Yoxtheimer, D., Pollak, J., Wilderman, C., and Wen, T. (2018). Engaging over data on fracking and water quality. Science *359*, 395–397.
- 7. Kim, B., Kwak, R., Kwon, H.J., Pham, V.S., Kim, M., Al-Anzi, B., Lim, G., and Han, J. (2016). Purification of High Salinity Brine by Multi-Stage Ion Concentration Polarization Desalination. Sci. Rep. *6*, 31850.
- 8. Lattemann, S., and Höpner, T. (2008). Environmental impact and impact assessment of seawater desalination. Desalination *220*, 1–15.
- 9. Vengosh, A., Jackson, R.B., Warner, N., Darrah, T.H., and Kondash, A. (2014). A Critical Review of the Risks to Water Resources from Unconventional Shale Gas Development and Hydraulic Fracturing in the United States. Environ. Sci. Technol. 48, 8334–8348.
- 10. Palomar, P., and Losada, I.J. (2011). Impacts of Brine Discharge on the Marine Environment. Modelling as a Predictive Tool (IntechOpen).
- 11. Wenten, I.G. and Khoiruddin (2016). Reverse osmosis applications: Prospect and challenges. Desalination *391*, 112–125.
- 12. Tong, T., and Elimelech, M. (2016). The Global Rise of Zero Liquid Discharge for Wastewater Management: Drivers, Technologies, and Future Directions. Environ. Sci. Technol. *50*, 6846–6855.
- 13. Greenlee, L.F., Lawler, D.F., Freeman, B.D., Marrot, B., and Moulin, P. (2009). Reverse osmosis desalination: water sources, technology, and today's challenges. Water Res. *43*, 2317–2348.
- 14. Ghaffour, N., Missimer, T.M., and Amy, G.L. (2013). Technical review and evaluation of the economics of water desalination: Current and future challenges for better water supply sustainability. Desalination *309*, 197–207.
- 15. Borsani, R., and Rebagliati, S. (2005). Fundamentals and costing of MSF desalination plants and comparison with other technologies. Desalination *182*, 29–37.
- 16. Sommariva, C., Hogg, H., and Callister, K. (2003). Cost reduction and design lifetime

- increase in thermal desalination plants: thermodynamic and corrosion resistance combined analysis for heat exchange tubes material selection. Desalination 158, 17–21.
- 17. Darwish, M.A., and Al-Najem, N.M. (1987). Energy consumptions and costs of different desalting systems. Desalination *64*, 83–96.
- 18. Ghaffour, N., Bundschuh, J., Mahmoudi, H., and Goosen, M.F.A. (2015). Renewable energy-driven desalination technologies: A comprehensive review on challenges and potential applications of integrated systems. Desalination *356*, 94–114.
- 19. Elimelech, M., and Phillip, W.A. (2011). The Future of Seawater Desalination: Energy, Technology, and the Environment. Science *333*, 712–717.
- 20. Tao, P., Ni, G., Song, C., Shang, W., Wu, J., Zhu, J., Chen, G., and Deng, T. (2018). Solar-driven interfacial evaporation. Nat. Energy *3*, 1031–1041.
- 21. Wang, Z., Horseman, T., Straub, A.P., Yip, N.Y., Li, D., Elimelech, M., and Lin, S. (2019). Pathways and challenges for efficient solar-thermal desalination. Sci. Adv. *5*, eaax0763.
- 22. Zhou, L., Tan, Y., Wang, J., Xu, W., Yuan, Y., Cai, W., Zhu, S., and Zhu, J. (2016). 3D self-assembly of aluminium nanoparticles for plasmon-enhanced solar desalination. Nat. Photonics *10*, 393–398.
- 23. Bae, K., Kang, G., Cho, S.K., Park, W., Kim, K., and Padilla, W.J. (2015). Flexible thin-film black gold membranes with ultrabroadband plasmonic nanofocusing for efficient solar vapour generation. Nat. Commun. *6*, 10103.
- 24. Zhou, L., Tan, Y., Ji, D., Zhu, B., Zhang, P., Xu, J., Gan, Q., Yu, Z., and Zhu, J. (2016). Self-assembly of highly efficient, broadband plasmonic absorbers for solar steam generation. Sci. Adv. 2, e1501227.
- 25. Zhang, L., Xing, J., Wen, X., Chai, J., Wang, S., and Xiong, Q. (2017). Plasmonic heating from indium nanoparticles on a floating microporous membrane for enhanced solar seawater desalination. Nanoscale *9*, 12843–12849.
- 26. Yi, L., Ci, S., Luo, S., Shao, P., Hou, Y., and Wen, Z. (2017). Scalable and low-cost synthesis of black amorphous Al-Ti-O nanostructure for high-efficient photothermal desalination. Nano Energy *41*, 600–608.
- 27. Ye, M., Jia, J., Wu, Z., Qian, C., Chen, R., O'Brien, P.G., Sun, W., Dong, Y., and Ozin, G.A. (2017). Synthesis of Black TiOx Nanoparticles by Mg Reduction of TiO2 Nanocrystals and their Application for Solar Water Evaporation. Adv. Energy Mater. 7, 1601811.
- 28. Zielinski, M.S., Choi, J.-W., La Grange, T., Modestino, M., Hashemi, S.M.H., Pu, Y., Birkhold, S., Hubbell, J.A., and Psaltis, D. (2016). Hollow Mesoporous Plasmonic Nanoshells for Enhanced Solar Vapor Generation. Nano Lett. *16*, 2159–2167.
- 29. Ni, G., Li, G., Boriskina, S.V., Li, H., Yang, W., Zhang, T., and Chen, G. (2016). Steam generation under one sun enabled by a floating structure with thermal concentration. Nat. Energy *1*, 1–7.
- 30. Li, Y., Gao, T., Yang, Z., Chen, C., Luo, W., Song, J., Hitz, E., Jia, C., Zhou, Y., Liu, B., et al. (2017). 3D-Printed, All-in-One Evaporator for High-Efficiency Solar Steam

- Generation under 1 Sun Illumination. Adv. Mater. 29, 1700981.
- 31. Kashyap, V., Al-Bayati, A., Sajadi, S.M., Irajizad, P., Wang, S.H., and Ghasemi, H. (2017). A flexible anti-clogging graphite film for scalable solar desalination by heat localization. J. Mater. Chem. A *5*, 15227–15234.
- 32. Zhao, F., Zhou, X., Shi, Y., Qian, X., Alexander, M., Zhao, X., Mendez, S., Yang, R., Qu, L., and Yu, G. (2018). Highly efficient solar vapour generation via hierarchically nanostructured gels. Nat. Nanotechnol. *13*, 489–495.
- 33. Heist, J.A. (1979). Freeze Crystallization. 15.
- 34. Bartholin, T., Haubold, P., Godicchen, M., and Bartholin, E. (1661). Thomae Bartholini de nivis usu medico observationes variae: accessit D. Erasmi Bartholini De figura nivis dissertatio; cum operum authoris catalogo (Typis Matthiae Godicchii, Sumptibus Petri Haubold, Bibl).
- 35. New experiments and observations touching cold, or, An experimental history of cold begun to which are added an examen of antiperistasis and an examen of Mr. Hobs's doctrine about cold / by the Honorable Robert Boyle ...; whereunto is annexed An account of freezing, brought in to the Royal Society by the learned Dr. C. Merret ... https://quod.lib.umich.edu/e/eebo/A29001.0001.001?view=toc.
- 36. www.bibliopolis.com Mundus Subterraneus, in XII Libros digestus... by Athanasius KIRCHER on JONATHAN A. HILL, BOOKSELLER, INC. JONATHAN HILL Books. INC. https://www.jonathanahill.com/pages/books/7681/athanasius-kircher/mundus-subterraneus-in-xii-libros-digestus.
- 37. Beier, N., Sego, D., Donahue, R., and Biggar, K. (2007). Laboratory investigation on freeze separation of saline mine waste water. Cold Reg. Sci. Technol. *48*, 239–247.
- 38. Khawaji, A.D., Kutubkhanah, I.K., and Wie, J.-M. (2008). Advances in seawater desalination technologies. Desalination *221*, 47–69.
- 39. Rich, A., Mandri, Y., Mangin, D., Rivoire, A., Abderafi, S., Bebon, C., Semlali, N., Klein, J.-P., Bounahmidi, T., Bouhaouss, A., et al. (2012). Sea water desalination by dynamic layer melt crystallization: Parametric study of the freezing and sweating steps. J. Cryst. Growth *342*, 110–116.
- 40. Cole, D.M., and Shapiro, L.H. (1998). Observations of brine drainage networks and microstructure of first-year sea ice. J. Geophys. Res. Oceans *103*, 21739–21750.
- 41. Williams, P.M., Ahmad, M., Connolly, B.S., and Oatley-Radcliffe, D.L. (2015). Technology for freeze concentration in the desalination industry. Desalination *356*, 314–327.
- 42. Fujioka, R., Wang, L.P., Dodbiba, G., and Fujita, T. (2013). Application of progressive freeze-concentration for desalination. Desalination *319*, 33–37.
- 43. Badawy, S.M. (2016). Laboratory freezing desalination of seawater. Desalination Water Treat. *57*, 11040–11047.
- 44. Xie, C., Zhang, L., Liu, Y., Lv, Q., Ruan, G., and Hosseini, S.S. (2018). A direct contact type ice generator for seawater freezing desalination using LNG cold energy. Desalination

- *435*, 293–300.
- 45. Raman, A.P., Anoma, M.A., Zhu, L., Rephaeli, E., and Fan, S. (2014). Passive radiative cooling below ambient air temperature under direct sunlight. Nature *515*, 540–544.
- 46. Chen, Z., Zhu, L., Raman, A., and Fan, S. (2016). Radiative cooling to deep sub-freezing temperatures through a 24-h day–night cycle. Nat. Commun. 7, 13729.
- 47. Incropera, F.P., and Incropera, F.P. eds. (2007). Fundamentals of heat and mass transfer 6th ed. (John Wiley).
- 48. Zhao, D., Aili, A., Zhai, Y., Xu, S., Tan, G., Yin, X., and Yang, R. (2019). Radiative sky cooling: Fundamental principles, materials, and applications. Appl. Phys. Rev. *6*, 021306.
- 49. Hossain, M.M., and Gu, M. (2016). Radiative Cooling: Principles, Progress, and Potentials. Adv. Sci. *3*, 1500360.
- 50. Li, W., Dong, M., Fan, L., John, J.J., Chen, Z., and Fan, S. (2021). Nighttime Radiative Cooling for Water Harvesting from Solar Panels. ACS Photonics *8*, 269–275.
- 51. Fournier, J., Grange, J.L., and Vergara, S. (1974). Water desalination by natural freezing. Desalination *15*, 167–175.
- 52. Mandal, J., Mandal, S., Brewer, J., Ramachandran, A., and Raman, A.P. (2021). Radiative Cooling and Thermoregulation in the Earth's Glow. ArXiv200611931 Phys.
- 53. Zhang, Y., Anim-Danso, E., Bekele, S., and Dhinojwala, A. (2016). Effect of Surface Energy on Freezing Temperature of Water. ACS Appl. Mater. Interfaces *8*, 17583–17590.
- 54. Chang, J., Zuo, J., Lu, K.-J., and Chung, T.-S. (2016). Freeze desalination of seawater using LNG cold energy. Water Res. *102*, 282–293.
- 55. Yang, Y., Lu, Y., Guo, J., and Zhang, X. (2017). Application of freeze concentration for fluoride removal from water solution. J. Water Process Eng. 19, 260–266.
- 56. Melak, F., Ambelu, A., Laing, G.D., and Alemayehu, E. (2017). Freeze Desalination as Point of Use Water Treatment Technology: A Case of Chromium (VI) Removal from Water. Proceedings *2*, 173.
- 57. Shirai, Y., Wakisaka, M., Miyawaki, O., and Sakashita, S. (1998). Conditions of producing an ice layer with high purity for freeze wastewater treatment. J. Food Eng.
- 58. Shirai, Y., Wakisaka, M., Miyawaki, O., and Sakashita, S. (1999). Effect of seed ice on formation of tube ice with high purity for a freeze wastewater treatment system with a bubble-flow circulator. Water Res. *33*, 1325–1329.
- 59. Luo, C., Chen, W., and Han, W. (2010). Experimental study on factors affecting the quality of ice crystal during the freezing concentration for the brackish water. Desalination *260*, 231–238.
- 60. Wang, P., and Chung, T.-S. (2012). A conceptual demonstration of freeze desalination-membrane distillation (FD-MD) hybrid desalination process utilizing liquefied natural gas (LNG) cold energy. Water Res. 46, 4037–4052.
- 61. Liu, L., Fujii, T., Hayakawa, K., and Miyawaki, O. (1998). Prevention of Initial Supercooling in Progressive Freeze-concentration. Biosci. Biotechnol. Biochem. 62,

- 2467-2469.
- 62. Wang, W., Shi, Y., Zhang, C., Hong, S., Shi, L., Chang, J., Li, R., Jin, Y., Ong, C., Zhuo, S., et al. (2019). Simultaneous production of fresh water and electricity via multistage solar photovoltaic membrane distillation. Nat. Commun. 10, 3012. 10.1038/s41467-019-10817-6.
- 63. Durkaieswaran, P., and Murugavel, K.K. (2015). Various special designs of single basin passive solar still A review. Renew. Sustain. Energy Rev. 49, 1048–1060. 10.1016/j.rser.2015.04.111.
- 64. Wang, P. (2018). Emerging investigator series: the rise of nano-enabled photothermal materials for water evaporation and clean water production by sunlight. Environ. Sci. Nano 5, 1078–1089. 10.1039/C8EN00156A.
- 65. Kaya, A., Tok, M.E., and Koc, M. (2019). A Levelized Cost Analysis for Solar-Energy-Powered Sea Water Desalination in The Emirate of Abu Dhabi. Sustainability *11*, 1691.
- 66. Cao, W., Beggs, C.B., and Mujtaba, I.M. (2015). Theoretical approach of freeze seawater desalination on flake ice maker utilizing LNG cold energy.
- 67. Akhtar, N., McGrath, L., and Roberts, P.D. (1979). Dynamic modelling and partial simulation of a pilot scale column crystallizer. Desalination 28, 1–11.
- 68. Orcutt, J.C., and Hale, F.J. (1970). The secondary refrigerant freezing process: A modeling study. Desalination 7, 201–227.
- 69. Williams, P.M., Ahmad, M., and Connolly, B.S. (2013). Freeze desalination: An assessment of an ice maker machine for desalting brines. Desalination *308*, 219–224.
- 70. Han, S., Shin, J.-Y., Rhee, Y.-W., and Kang, S.-P. (2014). Enhanced efficiency of salt removal from brine for cyclopentane hydrates by washing, centrifuging, and sweating. Desalination *354*, 17–22.
- 71. TROMBE, F. (1975). PERSPECTIVES SUR L'UTILISATION DES RAYONNEMENTS SOLAIRES ET TERRESTRES DANS CERTAINES REGIONS DU MONDE. Perspect. SUR Util. Rayonnem. Sol. Terr. DANS Certain. Reg. MONDE.